0038-075C/96/1619-616-632$03.00/0
Soil Science

September 1996
Vol. 161, No. 9
Printed in U.S.A.

THE WOLFFORTH FIELD EXPERIMENT: A WIND EROSION STUDY

John E. Stout and Ted M. Zobeck

The goal of this field study was to obtain a detailed account of wind erosion processes within a single agricultural field during a regional dust storm in the Southern High Plains of West Texas. The field, located in Wolfforth, Texas, was observed as the wind grew in strength, peaked, and later weakened. Sediment transport was monitored by an array of samplers spaced across the field, and meteorological information was obtained from a 10-m tower erected within the field. Erosion activity was monitored by a piezoelectric sensor that responded to the impact of saltating grains and provided a means for detecting the threshold of soil movement. Attempts were made to relate the observed temporal and spatial variations of sediment transport to meteorological factors and surface conditions. The results indicate that at the beginning of the storm, threshold was around 7 to 8 m/s. As the storm progressed, threshold appeared to slowly shift downward with time, suggesting a surface that was becoming increasingly erodible. Mass flux measurements showed substantial temporal variations that reflected changes of wind strength and changes in surface erodibility. The pattern of mass flux variation across the field was dependent on the height of measurement. The near surface flow of saltating grains ($z < 0.25$ m) was found to vary according to surface conditions, especially surface roughness. At greater heights, the flow of fine dust was less affected by surface conditions immediately beneath the point of measurement. Within the fully developed surface layer ($z < 0.25$ m), the mass flux profile was found to follow a modified power-law function. The near surface mass flux consisted of a broad range of particle sizes ranging from 50 μm to 300 μm, whereas farther from the surface the mode shifted distinctly toward smaller particle sizes with few particles larger than 100 μm. We show that it is possible to display graphically the relative contribution of the various grain sizes to the mass flux at each height in a way that makes it possible to visualize the zones of saltation and suspension, and the region of transition between these regimes.

WIND tunnels provide a controlled environment for the careful and systematic study of wind erosion processes, but there are important aspects of the wind erosion problem that are difficult to simulate in a wind tunnel. For example, field-scale variations of mass transport are difficult to study in the limited confines of a wind tunnel test section. Natural wind profiles, turbulence characteristics, and wind-direction fluctuations are also difficult to replicate in wind tunnel experiments. Thus, to obtain a true measure of wind erosion under natural atmospheric conditions and natural soil conditions, one must venture out to an actively eroding region and observe the wind erosion process in all its complexity.

Within this context we report here results from a wind erosion study within a farm field near Wolfforth, Texas. Our intention was to measure simultaneously as many different aspects of the wind erosion process as possible. We measured the dynamic nature of the wind fluctuations and their correlation with soil movement. We tried to better define the micrometeorology directly

USDA/Agricultural Research Service, Lubbock, TX 79401. Dr Stout is corresponding author. E-mail: jstout@mail.csrl.ars.usda.gov

[1] Names are necessary to report factually on available data; however, the USDA neither guarantees nor warrants the standard of the product, and the use of the name by USDA implies no approval of the product to the exclusion of others that may also be suitable.

Received Sept. 19, 1995; accepted April 18, 1996.

above the eroding field during the wind erosion event. We obtained measurements of mass flux across the field, and we attempted to correlate the spatial variations of sediment mass transport with measured soil surface conditions such as surface roughness, the availability of loose erodible material, and topography. We obtained measurements of mass flux at various heights above the field and we attempted to define the variation of the particle size distribution with height. We did not expect this experiment to yield fundamental mathematical relationships; rather we hoped that it would provide a glimpse of wind erosion under realistic conditions, and we hoped that it would point toward areas of future research.

PAST FIELD WORK

A considerable portion of past field work has focused specifically on blowing sand associated with vast sand sheets in desert regions. Much of this work has been summarized in comprehensive books written by Bagnold (1941) and Greeley and Iversen (1986). Large desert regions often lack well-defined erodible boundaries so the effect of these boundaries on the horizontal variation of mass transport has been largely ignored in desert research. In eroding agricultural lands, field boundaries have a considerable influence on the wind erosion process, and their effects cannot be ignored. Mass transport across agricultural fields with distinct erodible boundaries has been measured by Chepil (1946), Stout (1990), and Fryrear et al. (1991). For the case of uniform surface conditions, mass flux measured at a fixed height was found to increase with distance across the field until it asymptotically approached a limiting value called the transport capacity (Stout 1990). Chepil (1946) suggested that the rate of increase is strongly influenced by surface conditions such as roughness, soil type, and availability of loose material. Stout (1990) established that the rate of increase and the final limiting value of mass flux depended strongly on the height of measurement. Mass flux within the saltation zone was shown to more quickly reach transport capacity compared with the flux of fine dust grains moving farther from the surface.

Past measurements of the vertical distribution of mass flux above an eroding soil surface suggest that mass flux is maximum near the surface and decreases rapidly with height. Despite many careful experiments, there is considerable disagreement on the mathematical description of the mass flux profile. Exner (1928) and White (1982) have used a simple exponential expression. Von Karman (1947), Gillette & Goodwin (1974), and Zobeck & Fryrear (1986) have used a simple power-law expression. Kawamura (1951) used an integral form of the Bessel function. Zingg (1953) and Fryrear et al. (1991) used a modified power-law form. Fryrear and Saleh (1993) and Wilson et al. (1993) have used a combination of the power-law and exponential functions. Clearly, the mass flux profile is an important fundamental aspect of the wind erosion process that is still imperfectly understood.

A number of experiments in the past were designed to establish the threshold condition for soil movement. Many of these experiments were conducted in wind tunnels (Bagnold 1941; Chepil 1945b; Kawamura 1951; Zingg 1953; Nickling 1988). Typically, a soil surface is transplanted from the field into the test section of a laboratory wind tunnel, the wind speed is adjusted, and the critical wind speed at which soil movement is initiated is noted. The determination of threshold under natural field conditions is considerably more challenging, yet field investigations have been undertaken, and reasonable estimates of threshold have been obtained by Chepil (1945b), Svasek and Terwindt (1974), Gillette et al. (1982), Fryrear et al. (1991), and Gillette et al. (1995).

There have been several field investigations of the physical characteristics of blowing soil. Chepil (1945a) used a two-stage sediment sampler designed to separate saltating soil particles from those moving in suspension. Although the exact separation criterion was not well defined in this paper, Chepil effectively showed the relative proportion of soil carried in saltation and suspension at various heights above the eroding soil surface. This work did not provide useful information regarding the grain-size distributions at different heights above an eroding surface. Chepil (1957) and Chepil & Woodruff (1957) investigated the grain-size distributions of blowing dust at heights greater than 0.6 m, well above the saltation zone. Sediment samples were obtained by Nickling (1983) at heights greater than 0.5 m. Gillette & Walker (1977) compared the size distributions at 0.013 m, 1.0 m, and 1.5 m. They concluded that the size distribution close to the surface closely reflects the availability of particles within the parent soil, and they observed a distinct change of the particle size distribution from 0.013 m to 1.0 m. The lack of additional measurements between 0.013 m and 1.0 m precluded the complete description of the transition between these regimes. Leys and McTainsh (1994) measured the particle

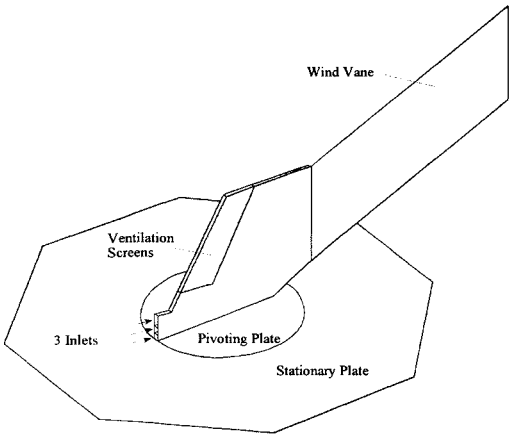

Fig. 1. Near-surface sampler used to measure sediment mass flux close to the eroding surface. This instrument has three inlets for measuring mass flux at three separate heights within 20 mm from the eroding surface. The inlets channel sediment to a container located beneath the ground. The sampler pivots to point into the wind. Ventilation screens aspirate the sampler and allow it to sample under near-isokinetic conditions.

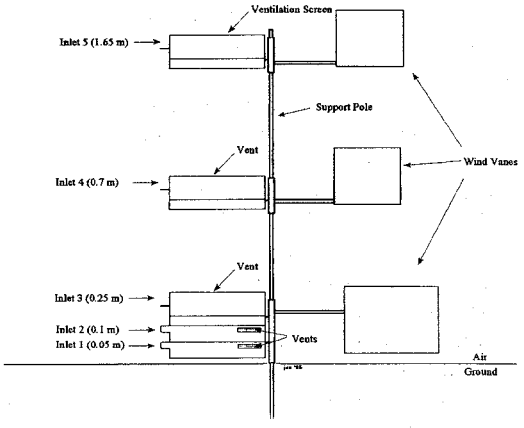

Fig. 2. BSNE sampling cluster used to measure sediment flux at five heights. The samplers are mounted on a support pole, and a wind vane aligns them with the wind. Each sampler has a separate inlet and ventilation screen.

size distribution at heights of 0.07 m, 0.25 m, and 2.0 m and showed that the mode size decreases systematically with height. Zobeck and Fryrear (1986) measured the particle size distribution of soil particles sampled at five heights between 0.15 m and 2.0 m. They showed that the fraction of sand-sized particles decreased smoothly with height.

FIELD EXPERIMENT

The experiment was conducted on April 14, 1994, within an eroding agricultural field in Wolfforth, Texas, near Lubbock. The soil type was a fine sandy loam with 15.1% clay, 11.4% silt, and 73.5% sand. Organic matter content was 0.34% with no carbonates. The site had been planted to wheat, but because of drought conditions and a previous wind erosion event, the young plants had been damaged. Emergency tillage involving a chisel was the last tillage operation on the field, and it produced a series of chisel tracks with their long axes running North-South. Weathering and deposition from previous blowing events had filled the chisel tracks so that they were ineffective in reducing wind erosion. We chose to measure wind erosion in the field in exactly the condition that the farmer left it rather than modify the field to produce ideal uniform conditions. As a result, surface properties, such as roughness and texture, varied across the field, especially near field boundaries.

We used two separate sampler designs to measure the full mass flux profile. We used a near-surface sampler to obtain measurements within the lowest 20 mm and a BSNE (Big Spring Number Eight) sampling cluster for higher heights. The near-surface sampler, shown in Fig. 1, was based upon a design by Stout and Fryrear (1989) but modified to collect material from three heights within the first 20 mm from the surface. The first inlet extended from the surface to a height of 3 mm, the second extended from 3 to 9 mm, and the third extended from 9 to 20 mm. All inlets were rectangular and had a width of 5.5 mm. The near-surface unit is mounted on a turntable and is directed into the wind by a vane. Sampling inlets funnel sediment to a collection pan located beneath the surface. Fig. 2 shows the BSNE sampling cluster used to measure sediment flux at heights greater than 20 mm. The BSNE samplers were developed by Fryrear (1986) and have been tested independently by Shao et al. (1993a). The sampling cluster consists of an array of five samplers each attached to a pivoting wind vane and each mounted at a different height on a central pole. Nominal sampling heights correspond to 0.05 m, 0.1 m, 0.25 m, 0.7 m, and 1.65 m. The nominal inlet areas are 200 mm^2 for the lowest two samplers and 1050 mm^2 for the upper samplers. The combination of the near-surface sampler

and the BSNE sampling cluster provides a total of eight sampling points above the eroding soil surface.

Despite their apparent differences, both the near-surface and the BSNE samplers are based upon the same operating principle. Sediment-laden air enters the sampler inlet and is slowed within the sampler by a diffuser section. Particles gravitationally settle into a collection pan located directly beneath the diffuser. Ventilation screens aspirate the sampler so that the inlet flow is nearly isokinetic (Stout & Fryrear, 1989). The mass of trapped soil is divided by the inlet area and the 1-h sampling time to obtain a time-averaged value of the horizontal component of sediment mass flux at each sampling height.

Spatial variations of mass flux were measured by six BSNE sampling clusters spaced horizontally across the field at x = 0, 34, 65, 124, 248, and 359 m, where x is the distance from the upwind edge of the field. Only one near-surface sampler was available, and it was placed near the fifth BSNE cluster at x = 248 m.

We used an instrument called SENSIT[1] to monitor saltation activity. SENSIT detects saltation activity by means of a piezoelectric crystal that responds to the impact of saltating grains and outputs a pulse signal proportional to the number of such impacts (Gillette and Stockton 1986; Stockton and Gillette 1990). SENSIT was buried as shown in Fig. 3 such that the lower edge of the sensing element was set flush with the eroding surface. The cylindrical sensing element extended from the surface to a height of 13 mm, and the diameter of the sensing element was 25 mm. We used the signal from SENSIT as a relative indication of erosion activity, and we made no attempt to interpret the signal as a quantitative measure of particle mass flux or momentum.

Micrometeorological information was monitored near the center of the field by a 10-m meteorological tower. The tower was mounted on a trailer and was designed to be towed behind a pickup truck. Once in position the tower was rotated quickly to its erect configuration. The tower was equipped with an array of temperature sensors, cup anemometers, a wind vane, a solar radiation sensor, and a relative humidity sensor. Anemometers were mounted at 0.2, 0.4, 1.0, 4.0, and 10.0 m, and the wind vane was placed next to the 10-m anemometer. The humidity sensor was mounted at 2 m. Temperature was measured at the soil surface (z = 0) and at heights of 0.2, 0.6, 1.0, 2.0, 4.0, and 10.0 m.

The meteorological tower was fully deployed by 09:00 local time on April 14, 1994, and we began to record wind profile data and wind erosion activity by 09:30. A continuous record of 1-minute average values of wind velocity, wind direction, temperature, relative humidity, and erosion activity was recorded from 09:30 to 18:30.

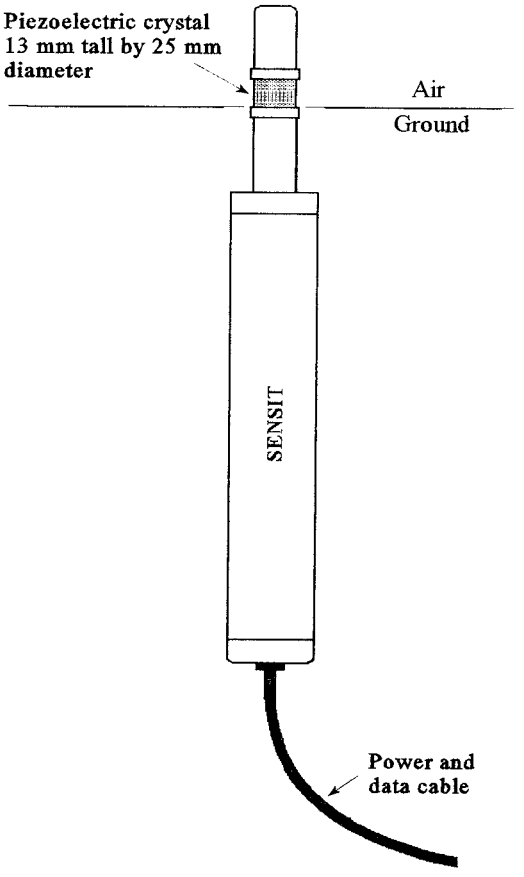

Fig. 3. SENSIT saltation sensor, which uses a piezoelectric crystal to detect particle impacts.

RESULTS AND DISCUSSION

Micrometeorology and Erosion Activity

What follows is a brief description of the overall storm dynamics as measured by our instrumentation. We will later describe and analyze the data in more detail but here we seek to describe the general nature of this wind erosion event.

The time history of the storm, as measured by our instrumentation, is plotted in Figs. 4 through 7. The 2-m temperature and relative humidity are

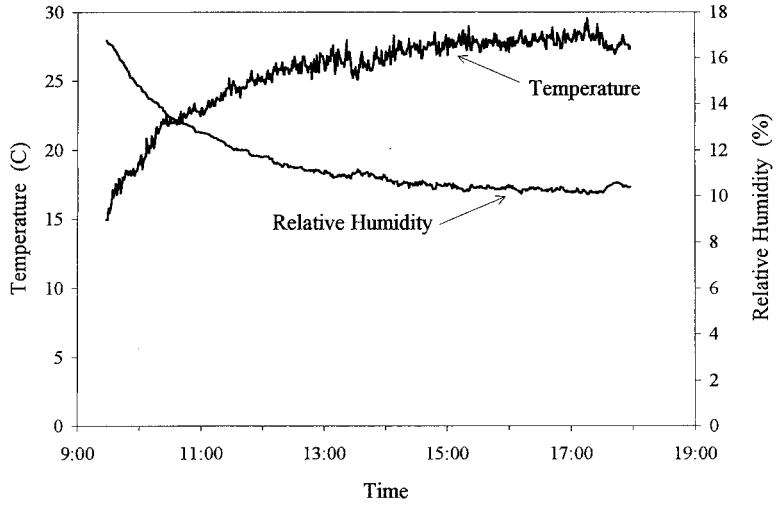

Fig. 4. Temperature and relative humidity measured at a 2-m height.

plotted in Fig. 4. Saltation activity, as measured by SENSIT, and the 10-m wind speed are plotted together in Fig. 5. Wind direction is plotted in Fig. 6, and temperature profiles are plotted in Fig. 7.

The results indicate a cool and calm morning with 2-m temperatures around 15° C, relative humidity of 17%, wind speeds around 5 to 6 m/s, and no detectable erosion activity. As the day progressed, conditions changed rapidly as winds increased in strength, temperatures increased, and relative humidity decreased. Around 10:30 a.m., the wind strengthened sufficiently to produce the first signs of wind erosion activity, as shown in Fig. 5. Intense blowing did not begin until about 12:30 and the strongest winds and erosion activity occurred from 14:30 to 16:00. By this time the 2-m air temperature had increased to around 28° C, relative humidity had dropped to 10%, and winds frequently gusted above 10 m/s. There were no major wind shifts during the experi-

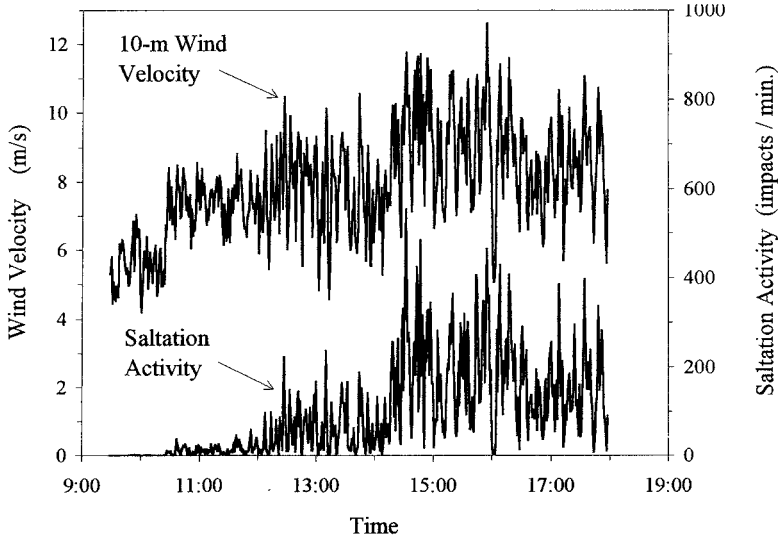

Fig. 5. Wind speed and saltation activity measured during the wind erosion event.

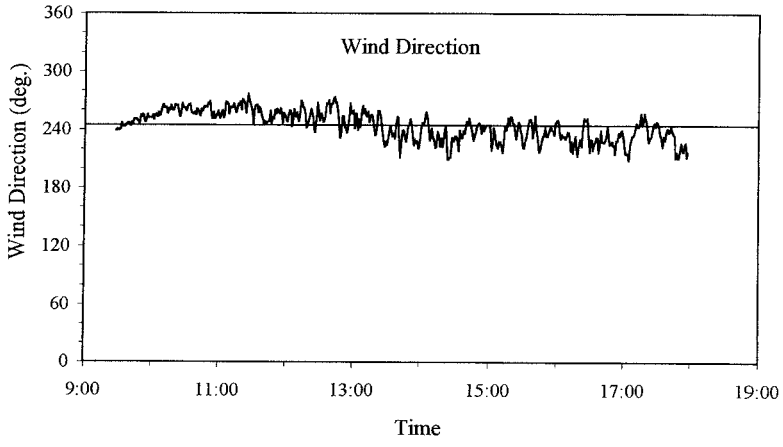

Fig. 6. Wind direction plotted as a function of time.

ment. As shown in Fig. 6, wind direction remained fairly constant, with a mean of 244° and a standard deviation of 14°. Wind strength and wind erosion activity declined significantly toward the end of the day.

Hourly-averaged temperature profiles, shown in Fig. 7, show a low-lying unstable layer beneath a height of 4 m in the early morning that later dropped to 2 m toward the end of the day. As the wind strengthened, strong turbulent mixing distributed the heat more uniformly throughout the boundary layer.

Threshold

It is difficult to see the relationship between wind speed and saltation activity clearly when these variables are plotted as a time series, as shown in Fig. 5. One alternative is to plot saltation activity as a direct function of wind velocity, thereby removing time as a variable (Fryrear et al., 1991; Gillette et al. 1995). The resulting scatter plots corresponding to each of the four 1-h sampling periods are shown in Fig. 8.

The scatter plots provide an interesting view of the response of the soil surface to wind gusts, and they also provide a means of estimating threshold velocity since non-zero SENSIT values indicate that winds exceed threshold. To obtain threshold we merely have to determine the lowest wind velocity at which saltation activity is first recorded.

Unfortunately this is not quite as easy as it sounds. Because of an imperfect correlation between wind forcing and saltation activity, it is often difficult to isolate a single representative value of threshold. Nevertheless, the scatter plot provides a good estimate of threshold. For example, during the first sampling period

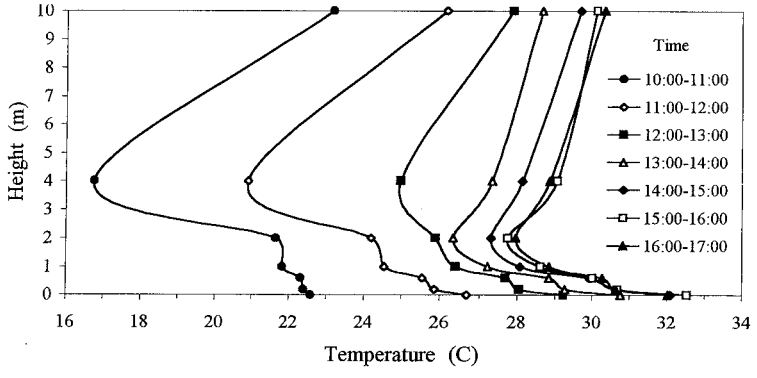

Fig. 7. Hourly averaged temperature profiles measured during the wind erosion event.

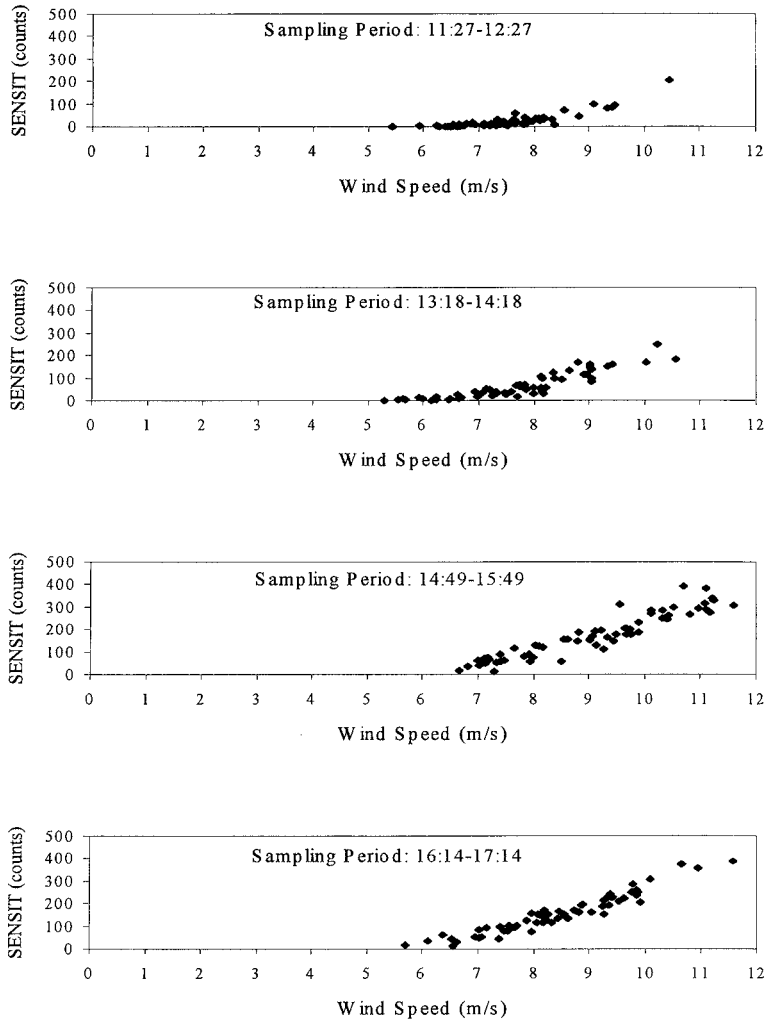

Fig. 8. Saltation activity plotted as a function of the 10-m wind speed for each 1-h sampling period.

(11:27–12:27), the surface was inactive when wind speeds were less than about 7 to 8 m/s, as shown in Fig. 8. During the second sampling interval, wind erosion was detected at considerably lower wind speeds of around 6 to 7 m/s. This downward trend was repeated in later sampling intervals and seems to indicate that the surface was becoming more erodible with time. This result agrees with Chepil's (1945b) observation that soil crusts tend to break down with time, thereby liberating underlying erodible fractions. Gillette et al. (1995) have also observed an increase in erodibility with time at Owens Lake, California, due to the breakdown of protective surface crusts.

Spatial Variation of Mass Flux

As mentioned previously, the spatial variation of mass flux was measured by an array of six BSNE sampling clusters spaced across the field.

TABLE 1

Hourly averaged 10-m wind speed and wind direction

Sampling interval	10-m Wind speed (m/s)	Direction (deg.)
11:27 to 12:27	7.49	255
13:18 to 14:18	7.65	237
14:49 to 15:49	9.06	237
16:14 to 17:14	8.47	230

TABLE 2

Measured mass flux as a function of height z and fetch x for each sampling interval

Height	x (m)	Mass flux ($g\ m^{-2}\ s^{-1}$)			
		11:27-12:27	13:18-14:18	14:49-15:49	16:14-17:14
z=0.05 m					
	0	0.22	0.25	0.91	1.18
	34	0.56	0.24	0.93	0.55
	65	0.15	0.18	1.05	0.64
	124	3.21	16.55	43.63	24.97
	248	27.24	45.07	99.86	65.1
	359	3.01	4.52	23.16	18.95
z=0.1 m					
	0	0.07	0.08	0.46	0.48
	34	0.23	0.14	0.75	0.45
	65	0.11	0.14	0.75	0.45
	124	0.64	4.24	11.31	6.53
	248	6.1	10.42	26.11	16.77
	359	1.57	2.28	11.36	7.12
z=0.25 m					
	0	0.05	0.04	0.2	0.23
	34	0.1	0.06	0.47	0.27
	65	0.06	0.09	0.45	0.3
	124	0.17	1.06	2.88	1.63
	248	0.92	1.83	4.60	3.28
	359	0.64	0.9	3.91	2.29
z=0.7 m					
	0	0.01	0.02	0.04	0.09
	34	0.05	0.06	0.3	0.16
	65	0.03	0.05	0.24	0.15
	124	0.04	0.24	0.62	0.33
	248	0.16	0.33	0.89	0.57
	359	0.23	0.31	1.18	0.65
z=1.65 m					
	0	0.02	0.01	0.08	0.03
	34	0.03	0.03	0.12	0.1
	65	0.02	0.04	0.16	0.08
	124	0.1	0.1	0.29	0.14
	248	0.07	0.13	0.37	0.21
	359	0.11	0.11	0.54	0.27

We thus obtained the horizontal variation of sediment flux at five heights during four separate 1-h sampling periods. The average wind speed and direction for these sampling periods are presented in Table 1, and the measured mass flux values are presented in Table 2.

The pattern of mass flux variation across the field was strongly dependent upon the height of measurement. Near-surface measurements ($z \leq 0.25$ m), shown in Fig. 9, reveal that the first three sampling clusters were within a region of low erodibility. Beyond the third cluster, near-surface measurements show a dramatic rise to a maximum mass flux near the fifth cluster at $x = 248$ m, followed by a sudden decrease at the end of the field. Farther from the surface ($z \geq 0.7$ m), shown in Fig. 10, we find that mass flux appears to increase continually with distance. This difference relates to the type of particle moving at different heights.

The lower samplers are primarily catching large grains that bounce along the surface in saltation. Since saltating grains frequently impact the surface, their motion is highly susceptible to changes of surface roughness. As shown in Fig. 11, measurements of surface roughness using the chain method (Saleh 1994) suggest higher values near field boundaries and a minimum roughness near the center of the field. The region of minimum roughness corresponds closely

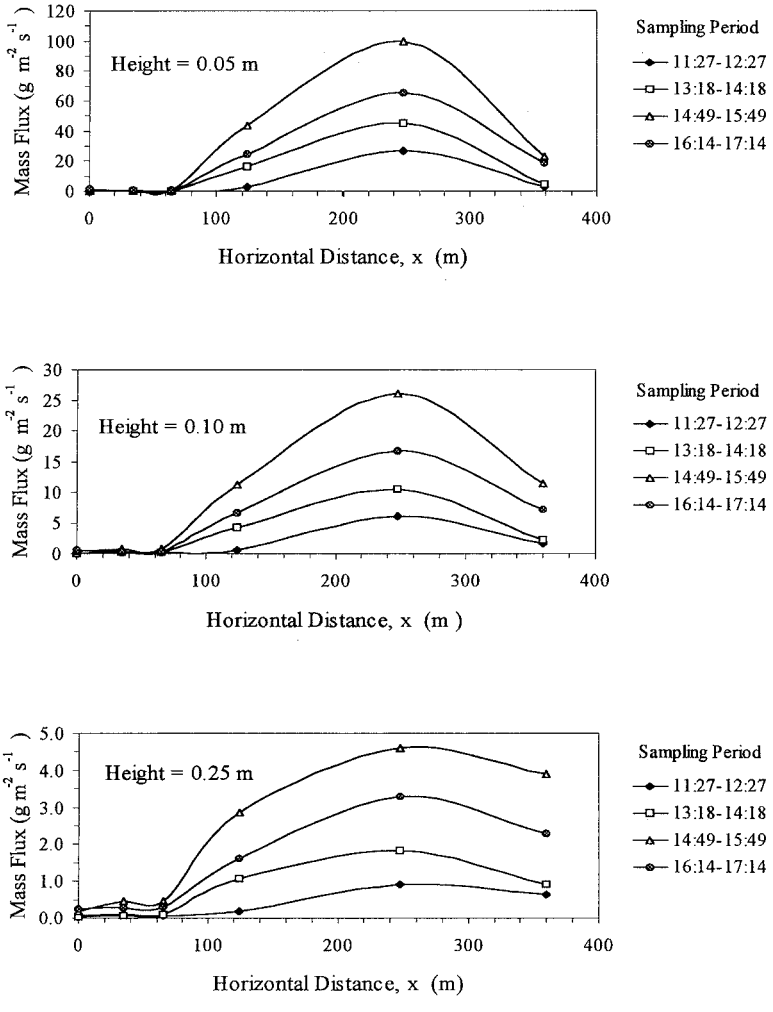

Fig. 9. Horizontal variation of sediment flux measured at heights of 0.05 m, 0.1 m, and 0.25 m.

to the region where the mass flux of saltating grains was maximum.

As shown in Fig. 12, measurements of the aggregate size distribution at three locations across the field reveal that the mass fraction of aggregates with diameter D less than 840 μm was maximum near the field center. The smooth curve, drawn in Fig. 12, may not be completely accurate because only three points were obtained over large horizontal distances. Nevertheless, the region of maximum mass flux appears to roughly match the portion of the field where the largest percentage of aggregates was of erodible size.

The field gradually sloped upward at an almost negligible slope of 1 m in 180 m, as shown in Fig. 13. There is a slight depression from x = 130 m to 250 m that may have in the past acted as a catchment for rainwater and associated runoff sediment. This may have contributed to the higher fraction of erodible-size aggregates in this vicinity.

Our results show that the maximum mass flux of saltating grains occurred just downwind of a slight topographic depression where surface roughness was minimum and the fraction of erodible-size aggregates was maximum. The large roughness near the upwind portion of the field retained particles by sheltering them from wind forces. Similarly, the large roughness at the downwind edge of the field effectively trapped a large fraction of the saltating grains before

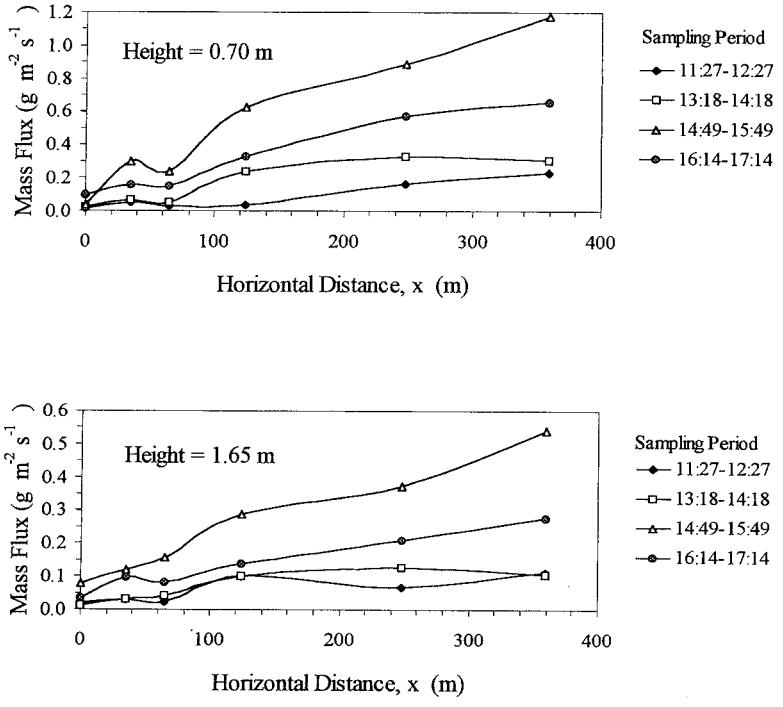

Fig. 10. Horizontal variation of sediment flux measured at heights of 0.70 m and 1.65 m.

they left the field. Samplers located well above 0.25 m were primarily catching fine dust moving in suspension, and because these fine grains rarely impact the surface, they were less susceptible to changes of surface conditions. As shown in Fig. 10, the magnitude of mass flux at heights well above 0.25 m increased continually with distance, although the surface roughness near field boundaries had trapped most saltating grains. One might expect the mass flux of suspension-size particles to level off or decrease if saltating grains are removed since it is generally believed that dust generation is intimately linked to the "splashing" of saltating grains into the bed (Shao et al. 1993b). However, dust grains are often initially entrained far upwind of the sam-

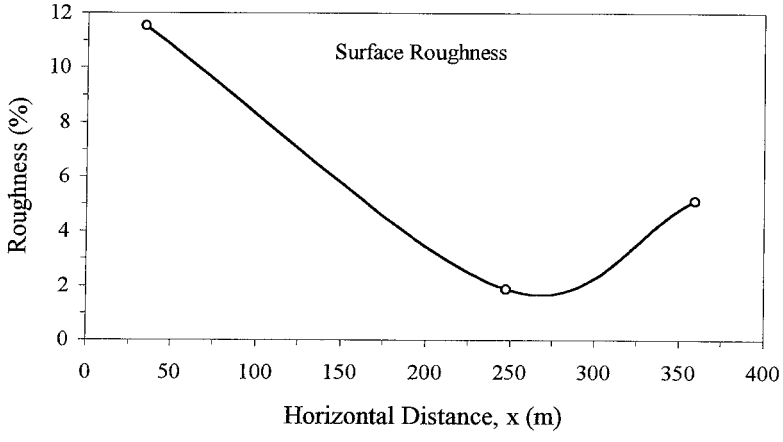

Fig. 11. Measurements of surface roughness using the chain method suggest higher values near field boundaries and a minimum near the center of the field.

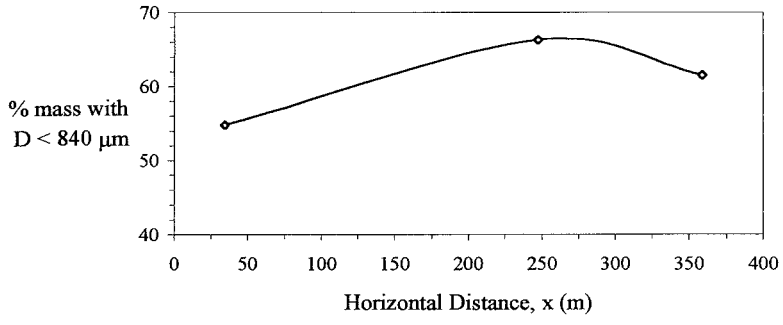

Fig. 12. Measurements of aggregate size distribution reveal that the mass fraction of aggregates with diameter (D) less than 840 μm was maximum near the field center.

pling point and may travel a considerable distance before they diffuse upward a few meters. Thus, the amount of fine dust often reflects the surface conditions upwind of the measurement point and not the surface directly beneath it. In fact, some of the fine dust captured in the upper samplers may have been generated in other fields.

In summary, measurements of mass flux show substantial spatial variability that depends on the height of measurement. Near-surface flow was controlled primarily by surface roughness that retains or traps saltating grains. Mass flow of suspension-size particles was less susceptible to surface conditions at the point of measurement but may reflect conditions upwind of the measurement point. Because saltating grains were trapped by roughness at the downwind edge of the field, only fine dust escaped field boundaries.

Temporal Variation of Mass Flux

As shown in Table 2, the maximum mass flux varied considerably between sampling periods. The lowest values occurred during the first sampling interval, between 11:27 and 12:27, as shown in Fig. 9. During the following hour, mass flux was nearly twice that of the first sampling interval although the mean wind speed, as shown in Table 1, was only slightly higher. This may indicate that the hourly-average wind speed is not the best indication of wind strength since it does not reflect the effects of strong intermittent wind gusts properly. Another possible explanation for this large increase in mass flux resulting from such a small change in wind speed may be change of surface erodibility. Chepil (1945b) observed such an increase in erodibility and attributed this change to the breakdown of a thin protective crust as a result of abrasion by saltating grains. Gillette et al. (1995) also observed a similar change of erodibility with time during experiments at Owens Lake, California. As crusts disintegrate and lose their protective value, underlying erodible particles are liberated and the supply of erodible material is increased. In addition, the gradual breakdown of surface clods and crust yields particles of erodible size,

TABLE 3

The measured fraction of mass flux P(z, D) at each height z contributed by particles that are smaller than a given size D for x = 248 m and time period 1449–1549.

z (mm)	Mass flux ($g\ m^{-2} s^{-1}$)	P (z, D)					
		45 μm	63 μm	90 μm	125 μm	250 μm	500 μm
1.3	739.69	0.00591	0.0300	0.1732	0.3827	0.8980	0.9912
5.9	573.67	0.00497	0.0219	0.1424	0.3537	0.9104	0.9925
15	244.07	0.00741	0.0268	0.1592	0.3836	0.9405	0.9974
45	99.86	0.00478	0.0353	0.1797	0.4023	0.9246	0.9976
95	26.11	0.0181	0.0727	0.2436	0.4246	0.9104	0.9989
245	4.597	0.0531	0.02228	0.5290	0.6694	0.9118	0.9976
695	0.888	0.1370	0.4618	0.8821	0.9680	0.9932	0.9992
1645	0.371	0.2139	0.5887	0.9416	0.9915	0.9994	1.000

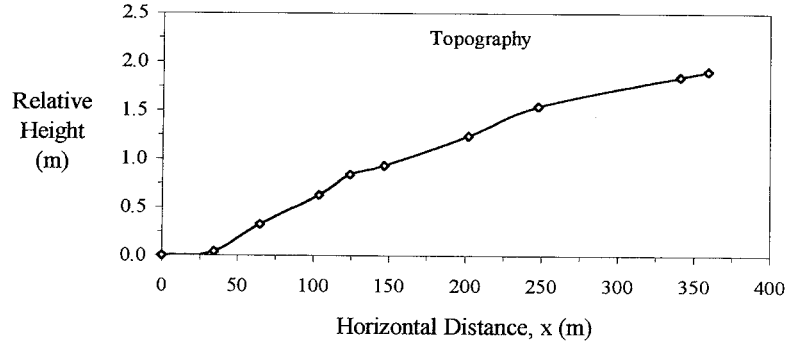

Fig. 13. Measurements of topography across the field show a gradual upward slope of 1:180 and a slight depression near the center of the field.

which then increases the supply of erodible grains. Thus, the supply of material available for transport may have increased significantly between the first and second sampling interval although the mean wind speed remained fairly constant.

The maximum flux rates occurred during the third sampling interval, between 14:49 and

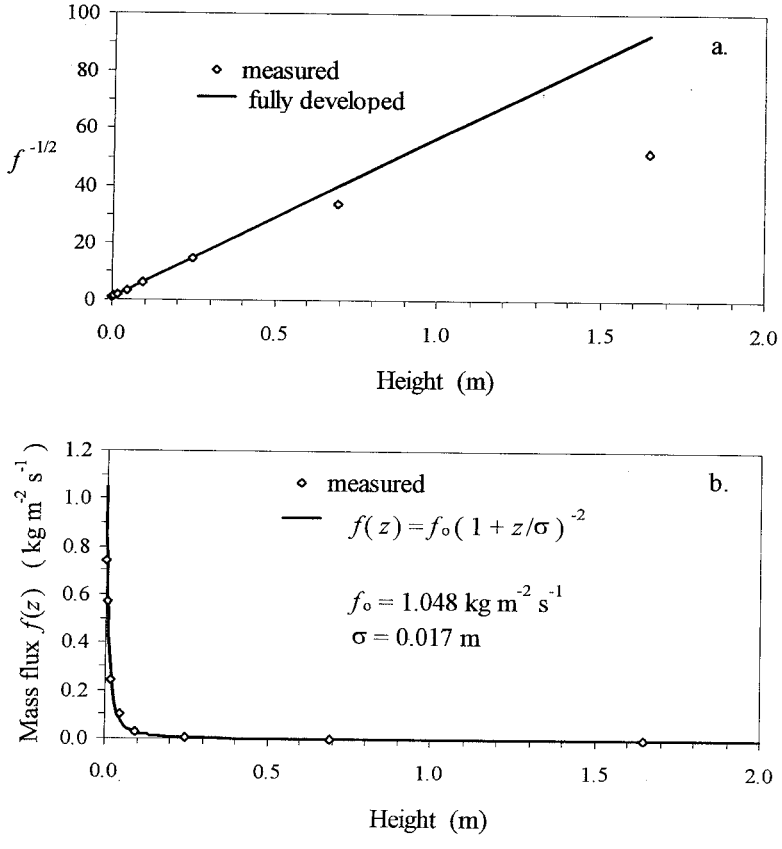

Fig. 14. (a) Values of the inverse square root of mass flux show a linear dependence on height within the fully developed portion of the profile. (b) A plot of the mass flux profile along with the power-law form of the flux profile equation at x = 248 m.

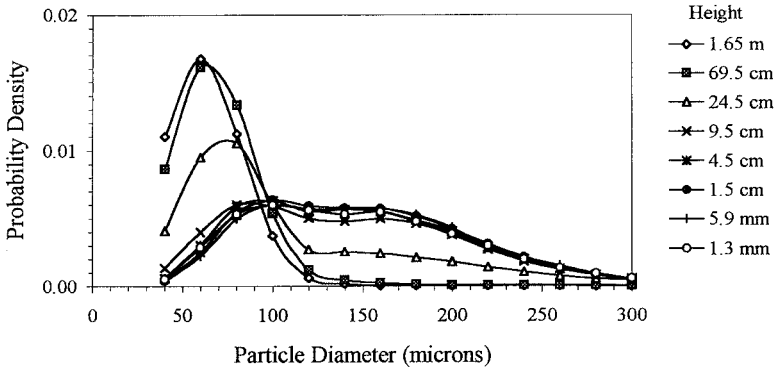

Fig. 15. Particle size distribution plotted at various heights.

15:49, as shown in Fig. 9. The average wind speed was significantly higher during this interval than at any other time, and it appears that there was an ample supply of loose erodible material.

Mass Flux Profile

Given sufficient distance and uniform conditions, mass flux measured at constant height will asymptotically approach a maximum value called the transport capacity. It has been found experimentally that the distance required to reach transport capacity increases with height (Stout 1990). Most fields are too short for transport capacity to be reached at all heights, but there is often a "fully developed" surface layer within which the mass flux profile is stable. Above this surface layer, mass flux values are still increasing with distance across the field and, therefore, the values are not yet stable.

The mass flux profile within the fully developed surface layer may be described by a simple power-law function of the form:

$$\frac{f(z)}{f_o} = (1 + \frac{z}{\sigma})^{-2} \qquad (1)$$

where $f(z)$ is the horizontal mass flux at height z, f_o is the mass flux at the surface ($z = 0$), and σ is a scale height. The form of Eq. (1) is a modification of the empirical equation used by Zingg (1953). Reworking Eq. (1) yields the linear form:

$$f(z)^{-1/2} = f_o^{-1/2}\left(1 + \frac{z}{\sigma}\right) \quad . \qquad (2)$$

Plotting values of $f^{-1/2}$ as a function of height, we find that values within the fully developed portion of the mass flux profile fall along a straight line.

As shown in Fig. 14a, measured flux values below a height of about 0.25 m appear to form a straight line at x = 248 m. Thus, at this position in the field, the fully developed surface layer is limited to this height. Linear regression of Eq. (2), using only the lower six points within the fully developed surface layer, we find that f_o = 1.048 kg m^{-2} s^{-1} and σ = 1.7 cm. A plot of the mass flux profile along with Eq. (1) is shown in Fig. 14b. Clearly, the mass flux profile within the surface layer is well represented by this power-law form. The results show that mass flux decreases rapidly with height. For example, mass flux at a height of $z = \sigma$ or 1.7 cm, reduces to 25% of the surface value. Integrating Eq. (1) from the surface to the height $z = \sigma$, we find that 50% of the total mass flow passes beneath the scale height σ. For this reason the scale height σ may be referred to as the "mean saltation height" (Bagnold 1941; Wilson 1994). Although the value of the mean saltation height may seem small, our result of 1.7 cm is supported by a large body of evidence. Past work starting from the pioneering work of Bagnold (1941) to more recent research by Anderson and Haff (1988), Butterfield (1991), Wilson (1994), Singh (1994), Neuman and Nickling (1994) support our finding that 50% of the mass flow passes beneath a height of a few centimeters.

Particle Size Distributions

Windblown sediment moving above an eroding soil surface consists of particles of different

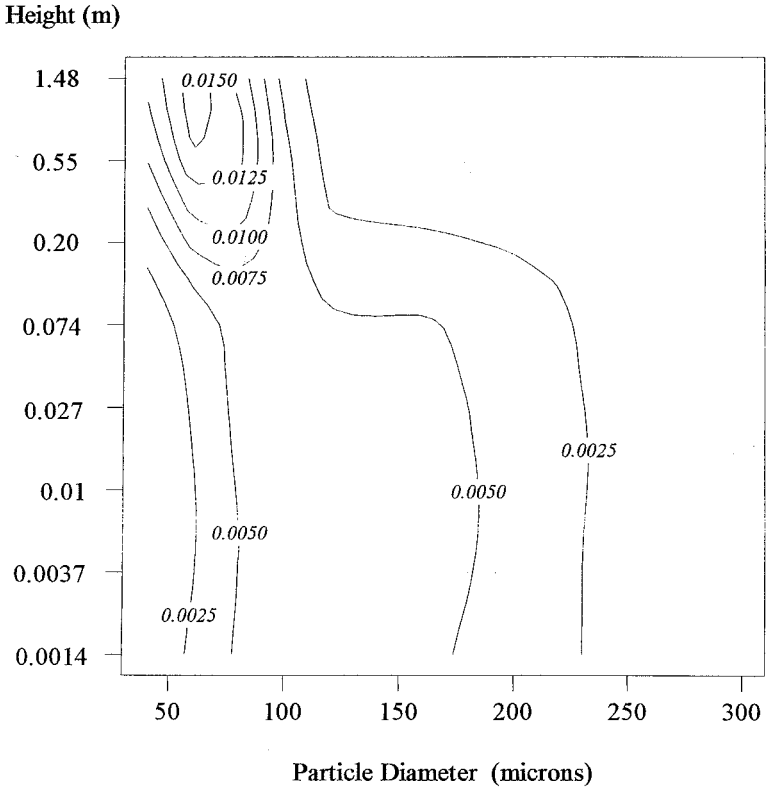

Fig. 16. Contour plot of the probability density p(z,D) shows how the particle size distribution varies with height.

sizes. If one were to sample material transported at a given height and then separate this material into discrete particle size ranges, one could ascertain the fraction of the total mass flux contributed by each size class. Since particle size is linked to the mode of transport, we could then estimate the relative contribution to the total mass flux of particles moving in saltation or suspension at each height.

During the transport of mixed sediments, large particles moving in saltation represent the dominant mode of transport near the surface. Since the top height of saltating grains is limited, small dust particles moving in suspension dominate transport far from the eroding surface (Chepil 1945a; Gillette and Walker 1977; Leys & McTainsh 1994). It is difficult to place definite limits on the boundary between the zone of saltation-dominated flow and the zone of suspension-dominated flow; particle motion gradually transitions from one regime to another.

Sediment collected at each sampling height z was sieved to determine the fraction of total mass P(z, D) with particle diameters less than a given size D. The sieve breaks were 45, 63, 90, 125, 250, and 500 μm. The results of this analysis are shown in Table 3. Each value of the cumulative distribution P(z, D) is equivalent to the fraction of the total mass flux at height z contributed by particles smaller than a given size D.

Our goal was to obtain, at each height z, the fraction of mass flux associated with a given particle size D. This is represented by the probability density function, denoted here by lower case p(z, D). The probability density is obtained by taking the partial derivative of the cumulative distribution function with respect to particle diameter. The probability density is calculated numerically as:

$$p(z, D) = \frac{\partial P}{\partial D} \approx \frac{P(z, D + \Delta D) - (P(z, D - \Delta D)}{2\Delta D} \quad (3)$$

Numerical error of this calculation is proportional to ΔD^2 so it is important to maintain a small step ΔD. As mentioned previously, the spacing between sieves was neither uniform nor small. Thus, it was necessary to generate a series of

more closely spaced extrapolated values of cumulative probability between measured values so that it was possible to obtain accurate numerical differentiation. A smooth curve was drawn through the measured values of cumulative probability, and points were generated to fill the gaps between the measured values at uniformly spaced increments of $\Delta D = 20$ μm. Then Eq. (3) was used to calculate values of probability density at increments of 20 μm at each measurement height. The results are plotted in Fig. 15.

The results show a fairly broad and uniform distribution near the surface ($z \leq 9.5$ cm) where the probability of finding a 80 μm particle is nearly identical to the probability of encountering a 180-μm particle. The distributions from 1.3 mm to 9.5 cm are nearly coincident, indicating that the distributions are independent of height within this near surface saltation zone. From $z = 9.5$ cm to $z = 24.5$ cm, a distinct transition occurs as one leaves the low-lying saltation cloud and enters the suspension zone. Above this transition region, the mode of the distribution shifts distinctly to smaller particle sizes, and the distribution is considerably more peaked.

We can clearly see this transition if we plot the probability density as a contour plot. Since $p(z, D)$ depends on two variables, we can plot the probability density function with particle diameter D on the horizontal axis and height z on the vertical axis. To obtain a reasonably good plot it was necessary to extend the resolution in the vertical direction. We chose to plot regular intervals of $\ln(z)$ rather than z since this shows the near-surface region with better clarity. To obtain values of $p(z,D)$ at regular intervals of $\ln(z)$, we again extrapolated between measured values. The original sampling heights were spaced close to uniform increments of $\ln(z)$, thus, the vertical extrapolation was not difficult.

The results, shown in Fig. 16, show clearly the grain-size characteristics of transported particles above this eroding mixed-sediment surface. Although this graphical approach was not expected to define the exact boundary between the saltation and suspension regimes, the results appear to depict these two regimes and the transition region between them. Near the surface, we find that the mass flux is dominated by large saltating grains. Farther from the surface, sediment flux is dominated by smaller particles moving in suspension. In the suspension-dominated zone, the mode appears to shift to smaller particle size with increasing height, whereas in the saltation zone the mode is independent of height.

At a height between 0.1 and 0.2 m, there exists a transition zone between the saltation-dominated zone and the suspension-dominated zone. As expected, this transition is smooth and gradual.

CONCLUSIONS

The purpose of this experiment was to observe wind erosion within a farm field in the semiarid high plains of West Texas. This experiment provided only a snapshot of field-scale wind erosion within a single field, during a single wind erosion event. Much more work is required to fully understand the many intricate relationships between the surface, soil, and wind.

By using a piezoelectric sensor to detect saltation activity, it was possible to establish the threshold wind speed at which soil movement was initiated. Our results indicate that for this soil surface, threshold was initially around 7 to 8 m/s, and it appeared to shift slowly downward with time, indicating a surface that was becoming more erodible.

This field experiment has added to our knowledge of the possible spatial variability within a complex field. Measurements at various heights across the field reveal that spatial variability of mass flux depends strongly on the height of measurement. The near-surface flow of saltating grains was controlled primarily by surface roughness. Here, the flow of saltating grains was found to increase initially from the erodible boundary, only to be trapped by surface roughness at the downwind portion of the field. The mass flow of suspension-size particles was less susceptible to surface conditions. The flow of fine dust increased steadily with distance across the field, although most of the saltating grains had been trapped by surface roughness near field boundaries.

The near-surface portion of the mass-flux profile was found to respond more quickly to surface conditions and became fully developed before the upper portion of the profile. Here, the fully developed surface layer was found to extend to a height of 0.25 m at $x = 248$ m. The mass flux profile within the stable surface layer was found to follow a modified power-law function that decreased rapidly with height. Integrating this power-law function, we find that 50% of the total mass flow passed beneath a height of 1.7 cm.

A method was developed to map the grain size characteristics of windblown sediment above a wind-eroding surface. Plotting the probability density as a contour plot with particle diameter along the horizontal axis and height along the

vertical axis, we form an interesting view of the contribution of various particle sizes to the mass flux at different heights. This graphical method clearly depicts zones of saltation-dominated flow, suspension-dominated flow, and the transition region between these zones. Here, saltation-dominated flow was found below a height of 0.1 m, a transition region occurred between 0.1 m and 0.2 m, and suspension was the dominant mode of transport above 0.2 m. Certainly, a different field with different soil conditions will yield a different map of physical characteristics; however, this graphical method could be used in any field where measurements are available.

ACKNOWLEDGMENTS

The authors acknowledge the hard work of H. Dean Holder, who constructed much of the equipment used in this experiment. We also thank the other team members that ventured into the raging dust storm to obtain the samples reported here: Dr. Jim Gregory, H. Dean Holder, Dr. Udai Singh, Bill Snyder, and Dr. Greg Wilson. In addition, we would like to thank Walt Haygood for allowing us to use his field for this experiment.

REFERENCES

Anderson, R. S., and P. K. Haff. 1988. Simulation of eolian saltation. Science 241:820–823.

Bagnold, R. A. 1941. The physics of blown sand and desert dunes. Methuen, London.

Butterfield, G. R. 1991. Grain transport in steady and unsteady turbulent airflows. Acta Mechanica (Suppl.) 1:97–122.

Chepil, W. S. 1945a. Dynamics of wind erosion: I. Nature of movement of soil by wind. Soil Sci. 60:305–320.

Chepil, W. S. 1945b. Dynamics of wind erosion: II. Initiation of soil movement. Soil Sci. 60:397–411.

Chepil, W. S. 1946. Dynamics of wind erosion: V. Cumulative intensity of soil drifting across eroding fields. Soil Sci. 61:257–263.

Chepil W. S. 1957. Sedimentary characteristics of dust storms: III. Composition of suspended dust. Am. J. Sci. 255:206–213.

Chepil, W. S., and N. P. Woodruff. 1957. Sedimentary characteristics of dust storms: II. Visibility and dust concentration. Am. J. Sci., 255:104–114.

Exner, F. M. 1928. Dünenstudien auf der Kurischen Nehrung. Sitzungsber. Mathem-naturw. Kl., Wien Ab. a 137:706–744.

Fryrear, D. W. 1986. A field dust sampler. J Soil Water Conserv. 41:117–120.

Fryrear, D. W., and A. Saleh. 1993. Field wind erosion: Vertical distribution. Soil Sci. 155:294–300.

Fryrear, D. W., J. E. Stout, L. J. Hagen, and E. D. Vories. 1991. Wind erosion: Field measurements and analysis. Trans ASAE, 34:155–160.

Gillette, D. A., and P. A. Goodwin. 1974. Microscale transport of sand-sized soil aggregates eroded by wind. J. Geophys. Res. 79:4080–4084.

Gillette, D. A., and T. R. Walker. 1977. Characteristics of airborne particles produced by wind erosion of sandy soil, High Plains of West Texas. Soil Sci. 123:97–110.

Gillette, D. A., J. A. Adams, D. Muhs, and R. Kihl. 1982. Threshold friction velocities and rupture moduli for crusted desert soils for the input of soil particles into the air. J Geophys Res 87:9003–9015.

Gillette, D. A., and P. H. Stockton. 1986. Mass, momentum and kinetic energy fluxes of saltating particles. *In* Aeolian geomorphology. W. G. Nickling (ed.). Allen and Unwin, Boston, pp. 35–56.

Gillette, D. A., G. Herbert, P. H. Stockton, and P. R. Owen. 1996. Causes of the fetch effect in wind erosion. Earth Surface Proc. Landforms 21: 641–659.

Greeley, R., and J. D. Iversen. 1986. Wind as a geological process on Earth, Mars, Venus, and Titan. Cambridge University Press, Cambridge.

Kawamura, R. 1951. Study on sand movement by wind. Institute of Science and Technology, Tokyo, Report 5, pp. 95–112.

Leys, J., and G. McTainsh. 1994. Soil loss and nutrient decline by wind erosion — Cause for concern. Aust. J. Soil Water Conserv. 7:30–35.

Neuman, C. M., and W. G. Nickling. 1994. Momentum extraction with saltation: Implications for experimental evaluation of wind profile parameters. Boundary-Layer Meteorol. 68:35–50.

Nickling, W. G. 1983. Grain-size characteristics of sediment transported during dust storms. Jr. Sed. Petrol. 53:1011–1024.

Nickling, W. G. 1988. The initiation of particle movement by wind. Sedimentology 35:499–511

Saleh, A. 1994. Measuring and predicting ridge-orientation effect on soil surface roughness. Soil Sci. Soc. Am. J. 58:1228–1230.

Shao, Y., G. H. McTainsh, and J. F. Leys. 1993a. Efficiencies of sediment samplers for wind erosion measurement. Aust. J. Soil Res. 31:519–531.

Shao, Y., M. R. Raupach, and P. A. Findlater. 1993b. Effect of saltation bombardment on the entrainment of dust by wind. J. Geophys. Res. 98:12719–12726.

Singh, U. B. 1994. Wind erosion: Mechanics of saltation and dust generation. Ph.D. Dissertation, Texas Tech University, Lubbock.

Stockton, P., and D. A. Gillette. 1990. Field measurements of the sheltering effect of vegetation on erodible land surfaces. Land Degrad. Rehabil. 2:77–85.

Stout, J. E., and D. W. Fryrear. 1989. Performance of a windblown particle sampler. Trans. ASAE 32: 2041–2045.

Stout, J. E. 1990. Wind erosion within a simple field. Trans. ASAE 33:1597–1600.

Svasek, J. N., and J. H. J. Terwindt. 1974. Measurements of sand transport by wind on a natural beach. Sedimentology 21:311–322.

Von Karman, T. 1947. Sand ripples in the desert. Technion Yearbook 6:52–54.

White, B. R. 1982. Two-phase measurements of saltating turbulent boundary layer flow. Int. J. Multiphase Flow 8:459–473.

Wilson, G. R., J. M. Gregory, T. M. Zobeck, and R. E. Zartman. 1993. Sediment transport by wind: A wind tunnel study. ASAE paper No. 932542.

Wilson, G. R. 1994. Modeling wind erosion: Detachment and maximum transport rate. Ph.D. Dissertation, Texas Tech University, Lubbock.

Zingg, A. W. 1953. Wind tunnel studies of the movement of sedimentary material. Proc. 5th Hydraulic Conf. Bull. 34:111–135.

Zobeck, T. M., and D. W. Fryrear. 1986. Chemical and physical characteristics of windblown sediment I. Quantities and physical characteristics. Trans. ASAE, 29:1032–1036.